# Ataxin-2 is essential for neurodevelopment in *Drosophila* and is a major regulator of the cytoskeleton.

Urko del Castillo*[1,a,b], Rosalind Norkett[1,a], Anna Serpinskaya[a], Vladimir I. Gelfand*[a]

a. Department of Cell and Developmental Biology, Feinberg School of Medicine, Northwestern University, Chicago, IL 60611.

b. Current address: Division of Hematology and Medical Oncology, Department of Medicine, Weill Cornell Medical Center, New York, NY, 10065.

*Urko del Castillo

*Vladimir I. Gelfand

1. These authors contributed equally to this work

**Email:** urd4002@med.cornell.edu, vgelfand@northwestern.edu

**Author Contributions:** UdC, RN and VG designed research, UdC, RN and AS performed research, UdC and RN analyzed data, RN, UdC and VG wrote the manuscript.

**Competing Interest Statement:** No competing interests.

**Classification:** Biological Sciences, Cell Biology

**Keywords:** Neuron, Microtubules, Actin, organelle trafficking.

**Abstract**

Ataxin-2 (Atx2) is a highly conserved RNA binding protein. Atx2 undergoes polyglutamine expansion leading to Amyotrophic Lateral Sclerosis (ALS) or Spinocerebellar Ataxia (SCA). However, the normal physiological functions of Atx2 remain unknown, likely because of functional redundancy between Atx2 and the related Atx2-Like gene in mammals. Here we use the powerful genetics of *Drosophila* to show that Atx2 is essential for normal cytoskeletal dynamics in neurons. Neuron-specific depletion of Atx2 caused multiple morphological defects in the nervous system of 3rd instar larvae. These include reduced brain size, impairments in optic lobe innervation and decreased dendrite outgrowth in sensory neurons. Defects in the nervous system of these larvae caused loss of the ability to crawl and were lethal at the pupal stage. Interestingly, we found severe impairments in cytoskeletal dynamics both in microtubule and actin networks. Microtubules became hyperstabilized as demonstrated by increased tubulin acetylation and resistance to microtubule depolymerizing drugs. Similarly, we found F-actin was hyperstabilized as shown by resistance to depolymerizing agents. Further, we show inhibition of microtubule-microtubule sliding, a crucial process for initial neurite outgrowth. We also demonstrated that microtubule-dependent transport of multiple cargoes in neurons, both *in vitro* and *in vivo*, was dramatically inhibited. Taken together, these data mark Atx2 as a master regulator of cytoskeletal dynamics and denote Atx2 as an essential gene in neurodevelopment, as well as a neurodegenerative factor. These data could provide insight into potential therapeutic interventions for Atx2 polyglutamine disorders.

**Significance Statement**

Neurons extend a complex array of axons and dendrites for network formation and communication. Therefore, precise neuronal development is essential for normal nervous system function and viability. Neuronal development is highly dependent upon dynamics of the actin and microtubule cytoskeleton for extension and maintenance of neurites. There are many descriptions of cytoskeleton impairment in neurodegenerative disease, however, the physiological functions of many genes mutated in neurodegenerative remain undescribed. The major finding of this work is

that the loss of Ataxin-2 at early developmental stages in *Drosophila* is lethal and causes multiple defects in neurodevelopment via dysregulation of the cytoskeleton.

## Main Text

### Introduction

Ataxin-2 (Atx2) is a highly conserved RNA binding protein which is known to associate with poly ribosomes, coordinate RNA granule assembly and regulate translation for synaptic plasticity (1–4). Atx2 contains mRNA binding domains, intrinsically disordered domains and a polyQ domain. This domain has been shown to undergo polyQ expansion leading to neurodegenerative diseases Spinocerebellar Ataxia (SCA) and Amyotrophic Lateral Sclerosis (ALS) (5, 6). SCA is characterized by decreased dendritic arbors and abnormal axons in the cerebellum (7), while ALS is characterized by motor neuron degeneration (8). Both conditions lead to movement disorders. Due to its causative role in neurodegenerative diseases, there has been much interest in discerning the function of Atx2, with research largely focused on the Atx2 polyQ expansion. However, Atx2 is expressed throughout development, indeed it is highly expressed in the developing central nervous system, and there have also been investigations focusing on the physiological roles of wild type Atx2. In one study, Atx2 knockout mice were generated (9). These mice displayed no obvious abnormalities, likely due to compensation by a related protein called Atx2-like. The gene encoding Atx2-like is absent in *Drosophila*, marking them as an ideal model organism to probe physiological Atx2 function.

Hints as to the physiological roles of Atx2 have come from studies of its domain structure (1, 10). Atx2 contains RNA binding domains and intrinsically disordered regions. Atx2 is known to associate with polyribosomes (11) and can assemble into phase-separated, membraneless stress granules, along with cognate RNAs. This action serves to concentrate or organize RNAs within the cell (12). In the case of Atx2, incorporation into phase separated stress granules is dependent upon the intrinsically disordered regions. Once assembled into granules, Atx2 can associate with its target RNAs, and stabilizes these transcripts (10). In turn, this action contributes to long term habituation or memory formation (1, 3). Via RNA organization and control of translation, Atx2 may be a critical regulator in many cellular pathways. For example, Atx2 has been previously indicated in actin regulation in the germline (4), microtubule organization in mitosis (13, 14), and in neurite outgrowth and ER distribution in neurons (15).

Here we use *Drosophila* to characterize the effects of neuron specific loss of wild type Atx2 on nervous system development. We show that depletion of Atx2 by RNAi at early developmental stages causes severe impairments in locomotion at the larval stage and is 100% lethal at the pupae stage of development. In affected larvae, we find impaired brain development and, at the cellular level, decreased neurite outgrowth of axons and dendrites. We probe the reasons behind these observations, both in *Drosophila* S2 cells as a versatile tool for protein knock down, and in *Drosophila* neurons. We show the microtubules are hyperacetylated and much less dynamic upon Atx2 knockdown. The actin cytoskeleton is similarly hyperstabilized. We further demonstrated that Atx2 loss causes a dramatic reduction in organelle transport in neurons in culture and *in vivo*. This leads to disturbed cargo distribution, with organelles becoming trapped in neurite varicosities. Within these varicosities, the microtubule cytoskeleton is highly disorganized, showing looping rather than linear microtubules. Together, our work describes that Atx2 is an essential gene in

neurodevelopment, required for proper cytoskeleton organization, dynamics and organelle transport.

**Results:**

**Ataxin-2 is essential for neurodevelopment, locomotion and viability in *Drosophila.***

We used the powerful genetics of *Drosophila* to probe the physiological roles of Atx2. In this way, we were able to take advantage of the presence of a single Atx2 gene, and avoid potential redundancy between mammalian Atx2 and Atx2-like (9). In order to study the physiological role of Atx2 in neurons, we depleted the protein by neuron specific expression of shRNA against Atx2 using the pan-neuronal driver elav-Gal4. Crucially, this is a post-mitotic driver, so any role for Atx2 in cell division is not affected.

We started by investigating the effect of neuron specific Atx2 depletion on the whole animal by looking at viability. We found that depleting Atx2 in neurons was lethal at the pupae stage and animals expressing the Atx2 RNAi were not viable to adult stages (Fig. 1A, control; 523/528, RNAi line 1; 0/458, RNAi line 2; 0/188 flies eclosed). We found consistent results with two different Atx2 RNAi lines; therefore, this effect is specific to Atx2 knockdown rather than an off-target effect. Atx2 knockdown was confirmed by western blot of brain lysate (Fig. S1). We also carried out locomotion studies. We imaged 3$^{rd}$ instar larvae crawling on agar plates and calculated the velocity. Control larvae crawled over the surface of the plate at about 0.7mm/s. However, Atx2 knockdown larvae were largely stationary, crawling with a velocity of less than 0.1mm/s (Movie 1). This is further shown by the color-coded tracks of each larva over time (Fig. 1B), and quantified in Fig. 1C.

We wanted to investigate the reasons behind these drastic effects of Atx2 depletion. We carried out experiments to study development of the nervous system. Firstly, we dissected 3$^{rd}$ instar larvae brains and immunostained for Fasciclin II (FasII) – an axon specific marker. We found that Atx2 RNAi brains were drastically smaller than controls. Quantification of the optic lobes (Fig. 1D, cyan) showed a roughly 2-fold decrease in area (Fig. 1E). Further we quantified area of the retinotopic pattern – the structure representing the photoreceptor axons (Fig. 1D, magenta). When normalized to the area of the optic lobe, we found this structure was decreased to around 10% of control area upon Atx2 depletion (Fig. 1F). These phenotypes demonstrate that Atx2 depletion induces impairment of axon outgrowth and targeting.

We investigated the effect of the loss of Atx2 on dendritic development. To do this, we labelled Class IV da (Dendritic arborization) neurons (sensory neurons that line the *Drosophila* body wall) with a fluorescent reporter expressed specifically in these cells (ppk::tdTomato). Under control conditions, these neurons extended long, branched dendritic arbors which covered the whole body segment. However, upon loss of Atx2, we found that these dendritic arbors were drastically shrunken (Fig. 1G). This effect was quantified in two ways, firstly the total dendrite length per cell was decreased around 65% (Fig. 1H). These observations are consistent with our previously published *in vitro* data where we showed depleting Atx2 decreased neurite length in cultured neurons (15). Secondly, to further describe the effect of Atx2 depletion on the shape of the dendritic arbor, we carried out Sholl analysis (16). This analysis describes dendritic complexity as a function of distance from the soma. Concentric circles are drawn outwards from the soma, and number of intersections that the dendritic arbor makes with each circle is counted. From 20µm from the soma, the Atx2 RNAi neurons displayed many fewer intersections than control neurons and the dendritic

arbors only extended to around 100µm from the soma, whereas the dendrites of the control neurons extended around 30% more than this (Fig. 1I). Therefore, the Atx2 knock down severely impairs dendrite development.

Taken together, these data show that Atx2 is necessary for normal development of both axons and dendrites. As a result, the loss of Atx2 severely impairs nervous system development and this causes severe locomotion defects and lethality.

**Ataxin-2 depletion decreases microtubule dynamics.**

We and others have demonstrated that one of the major drivers of neuronal development and neurite outgrowth is the microtubule cytoskeleton (17–21). An inability to properly regulate microtubule dynamics leads to phenotypes similar to those we reported upon Atx2 depletion (19). Therefore, we investigated the possibility that microtubule dynamics may be altered upon Atx2 knockdown. Initially, we chose to use *Drosophila* S2 cells to test this hypothesis as they are an efficient system to study the cytoskeleton using dsRNA strategies (22, 23). We depleted Atx2 in *Drosophila* S2 cells and carried out immunostaining for acetylated tubulin. Tubulin acetylation increases with microtubule age, so is a read out for microtubule lifetime (24–26). In S2 cells, we found a roughly 3-fold increase in acetylated tubulin signal (Fig. 2A, B). Importantly, this finding was also apparent in *Drosophila* 3$^{rd}$ instar larvae neuronal culture *in vitro*. Upon Atx2 knockdown with elav-Gal4, we found acetylated tubulin signal increased around 30% compared to control (Fig. 2C, D). Further, we investigated acetylated tubulin levels in brain lysate from elav>Atx2 RNAi larvae brains. Consistent with our immunostaining data, western blotting demonstrated an increase in acetylated tubulin in Atx2 RNAi brain lysate compared to control (Fig. 2E). Taken together, these results suggest an increase in microtubule stability upon loss of Atx2.

To investigate whether the increase in acetylated tubulin was related to an alteration in microtubule dynamics, we directly observed exchange of tubulin subunits – the building blocks of polymerized microtubules. To do this, we depleted Atx2 by RNAi in *Drosophila* S2 cells expressing photoconvertible EOS-tubulin. UV-light was applied to a specific region of interest and the photoconverted signal outside the original ROI was quantified 30 minutes after photoconversion. Incorporation of photoconverted tubulin subunits to microtubules located outside the original photoconverted area indicates tubulin subunit exchange. Under control conditions, around 50% of the original photoconverted signal was detected outside the ROI, whereas upon Atx2 depletion, this value was around 25% (Fig. 2F, G, movie 2). This indicates that Atx2 is necessary for normal subunit exchange. Additionally, we investigated the stability of microtubules after treatment with a microtubule depolymerizing agent vinblastine by immunostaining for tubulin. Consistent with our previous data, we found that Atx2 depletion confers resistance of microtubules to vinblastine – intact microtubules could be detected in the Atx2 RNAi cells, whereas microtubules in the control cells were largely depolymerized (Fig. 2H and I).

In order to directly assess the effect of loss of Atx2 on microtubule dynamics, we carried out live imaging of EB1 (end binding protein 1) – a marker for polymerizing microtubule plus-ends (27). Initially, we observed EB1-GFP comets in S2 cells (Fig. 2J and K, movie 3). We found around a 65% decrease in the number of comets per cell, as indicated by the loss in comets shown in the temporal color code – a color coded projection of each comet over time. Furthermore, we carried out the same assay in cultured larvae neurons expressing EB1-GFP (Fig. 2L, movie 4). Comets in neuronal processes are demonstrated in kymographs in Fig. 2M where time is projected on the Y axis, showing motile objects as diagonal lines. Upon Atx2 knockdown, we found a roughly 30%

decrease in the number of comets per 10µm (Fig. 2N). Notably, the total microtubule content in these cells is unchanged, as shown by tubulin staining of extracted control and Atx2 knockdown neurons (Fig. S2A, B). Therefore, Atx2 knockdown decreases only the dynamic microtubule population, not the total number of microtubules. Taken together, these data show that loss of Atx2 confers increased microtubule stability and that Atx2 is essential for normal microtubule dynamics, both in cultured S2 cells, and crucially, in neurons.

**Ataxin-2 depletion stabilizes the actin cytoskeleton**

In addition to the microtubule cytoskeleton, neuronal morphology is also dependent upon the actin cytoskeleton. Therefore, we decided to study the possibility that Atx2 depletion may impact actin dynamics. Initially, we knocked down Atx2 by RNAi in *Drosophila* S2 cells as a tractable system to study actin dynamics. We stained for actin filaments using Rhodamine-phalloidin. We also treated these cells with Latrunculin B (LatB), an actin depolymerizing agent, a comparable experiment to Fig. 2H. We found that in control cells, the F-actin signal, detected by phalloidin staining, was decreased by around 35%, indicative of actin depolymerization. However, upon Atx2 knock down, this effect was occluded. There was no significant alteration in F-actin signal (Fig. 3A, B). To make this observation relevant to neurodevelopment, we carried out similar experiments in cultured neurons from *Drosophila* 3$^{rd}$ instar larvae, either wild type, or after Atx2 knock-down. We demonstrated that after Atx2 knockdown actin filaments in neurons are more stable. As demonstrated by Rho-phalloidin staining about 40% more F-actin survived the treatment with LatB (Fig. 3C, D). LatB promotes depolymerization of F-actin by sequestering actin monomers. This shows that actin polymers are less sensitive to depolymerizing agents upon loss of Atx2, and so, that the actin network is less dynamic.

In order to study the potential effects of increased actin stability on neuronal morphology, we chose to observe filopodia, thin rod like protrusions rich in F-actin, essential for generation of neurites and the growth cone (28). We prepared primary neuronal cultures from 3$^{rd}$ instar larvae and carried out phase contrast imaging to examine filopodia along neuronal processes. Upon loss of Atx2, the number of filopodia projecting from neurites decreased over 50% (Fig. 3E, F). This is consistent with a less dynamic actin network upon loss of Atx2. Without correct actin dynamics, formation of filopodia is impaired and neurons are unable to extend normal arbors, consistent with our data showing that dendrite and axon development is affected by Atx2 loss (Fig. 1).

Taken together, these data show that Atx2 is essential for normal actin dynamics in neurons. These effects are comparable to our data demonstrating the microtubule network is stabilized upon Atx2 knockdown, and highlights the role of Atx2 in regulating normal cytoskeletal dynamics in neurons.

**Ataxin-2 is essential for organelle transport and distribution in *Drosophila* neurons**

Beyond neuronal morphology, both actin and microtubule networks are crucial for normal organelle transport. Microtubules act as tracks for longer range transport of cargo by kinesin and dynein motors, whereas actin is responsible for shorter range transport and cargo anchoring by myosin motors (29–33). Therefore, we hypothesized that Atx2 depletion may alter organelle transport via its effects on the cytoskeleton. To investigate the effect of loss of Atx2 on organelle trafficking, we started by carrying out live imaging of mitochondria and lysosomes in *Drosophila* 3$^{rd}$ instar larvae neurons in culture (Fig. 4A). Using the neuron specific driver elav-Gal4, we labelled mitochondria using a genetically encoded mCherry fluorescent protein targeted to the outer mitochondrial membrane. Time lapse microscopy showed around 45% of these organelles were motile in control conditions. However, depletion of Atx2 caused a large decrease in the fraction of motile mitochondria – only around 15% of mitochondria moved in the Atx2 RNAi condition, roughly 65%

less than in control neurons. This is exemplified in the kymographs in Fig. 4B and in movie 5 and quantified in Fig. 4D. In addition to mitochondria, we studied the motility of lysosomes labeled with lysotracker. Consistent with our data for mitochondrial transport, we found a vast decrease in lysosome motility upon loss of Atx2 (Fig. 4C, movie 6) – in control conditions around 30% of the organelles were moving, this dropped about two-fold in Atx2 RNAi neurons (Fig. 4E).

Next, we extended these findings to investigate organelle transport *in vivo* in the segmental nerves of *Drosophila* 3rd instar larvae. These nerves contain the axons of motor and sensory neurons which extend from the CNS into segments of the larvae body wall (Fig. 4F). The great advantage of this system is that the nerves are visible in the intact *Drosophila* larva without the need for dissection (34). We studied motility of two cargoes; mitochondria and dense core vesicles. We found that *in vivo* mitochondrial transport was drastically decreased in Atx2 RNAi animals compared to control, from around 50% of mitochondria moving to around 2% (Fig. 4 G, I, movie 7). Trafficking of dense core vesicles was similarly impaired in Atx2 RNAi larvae – motile organelles decreased from around 70% to around 20% (Fig. 4H, J, movie 8). Taken together these data show Atx2 has an essential role in normal organelle transport in neurons *in vitro* and *in vivo*, and that Atx2 is necessary for normal transport of multiple cargoes.

To study the effect of Atx2 dependent loss of cargo transport, we investigated the distribution of organelles throughout neurons in culture. We have previously shown that depleting Atx2 leads to varicosities in neuronal processes and that endoplasmic reticulum accumulates in these structures (15). Phase contrast imaging coupled with labelling of mitochondria and lysosomes demonstrated that these organelles could be found colocalized in the axonal varicosities (Fig. 4K). Indeed, the majority of the varicosities held both of these organelles (84%) while only around 5% each of varicosities contained only one or neither of these organelles. This is consistent with a 'traffic jam' leading to accumulation of organelles at these sites due to severely impaired transport.

Finally, we were interested in the microtubule structure at these 'traffic jam' sites. In order to visualize microtubules at the sites, we carried out super resolution imaging on extracted Atx2 RNAi neurons with stained for tubulin. We found that microtubules in these regions were less bundled, and instead were disordered and looped (Fig. 4L). This disorganization of the microtubule network is likely responsible for preventing normal organelle transport through these sites, causing their accumulation.

**Discussion**

Multiple works have demonstrated the involvement of mutant Atx2 in neurodegenerative conditions ALS and SCA (5, 6). However, an understanding of the physiological roles of the RNA-binding protein in neurons is lacking. Here we use *Drosophila* as a model system to effectively demonstrate the necessity of wild type Atx2 for normal nervous system development. Underlying the gross morphological defects seen in the nervous system, we show that loss of Atx2 has large scale effects on the microtubule and actin cytoskeleton, causing their abnormal stabilization. We also demonstrate that Atx2 is essential for normal organelle transport and distribution. These neurodevelopmental defects severely impair neurite outgrowth, locomotion of *Drosophila* larvae and are lethal at later stages of development.

Here we show that Atx2 is essential for normal cytoskeletal dynamics, in both microtubule and actin networks. Firstly, our data show that specific depletion of Atx2 in neurons drives an increase in microtubule acetylation, a decrease in tubulin subunit exchange and fewer EB1 comets. Thus, we conclude microtubules shift to a more stable, less dynamic network. A role for Atx2 in regulating

the microtubule network is consistent with previous reports of Atx2 having roles in centrosome organization and mitotic spindle regulation in *C. elegans* (13, 14). Secondly, we also found an increase in the stability of the actin network upon Atx2 knockdown. These data are in good agreement with early descriptions of Atx2 function, which showed evidence of disorganized actin bundles in retinal precursor cells, the female germline and bristles in Atx2 null *Drosophila* (4).

Microtubule and actin dynamics are intricately linked with neurite outgrowth. Microtubules not only serve as tracks for directed transport but they are crucial to transduce forces that are generated by molecular motors, which control neuronal polarization and morphology (18, 35–40). Therefore, it is highly likely that the developmental defects reported herein are dependent upon loss of microtubule dynamics. In neurons in particular, impaired actin dynamics have important consequences on development (41). Interrupting the actin network prevents normal growth cone formation, and so, normal axon outgrowth (28). Incorrectly regulated actin dynamics may also impair the organization of the microtubule cytoskeleton. Actin is necessary to guide microtubules in the axon, at filipodia and at the growth cone (42–45). Fewer filopodia being able to form may contribute to the decrease in dendritic branching described in DA neurons, potentially underlying the gross neurite extension defects we describe.

Finally, we show that decreasing levels of Atx2 decreases organelle transport in culture and *in vivo*. Impaired organelle transport is likely a direct consequence of the cytoskeletal defects caused by Atx2. This is supported by our observation of microtubule looping and disorganization in the axonal varicosities. The increase in microtubule stability and longevity would be thought to facilitate microtubule motor- based organelle transport (46, 47). However, we see a decrease in motility of multiple cargoes. Instead, an increase in the stability of the actin network may lead to organelles being anchored or trapped by myosin motors (30, 31). This loss of organelle transport leads to 'traffic jams' – an accumulation of organelles - in axonal varicosities. These axonal varicosities are also known to contain ER aggregates (15). In turn, this impairment in organelle distribution could lead to the neuronal defects we observed with loss of Atx2 at early developmental stages (39).Other examples of impaired organelle transport in neurodegenerative disease include mitochondria trapped in dystrophic neurites in an Alzheimer's disease model (48, 49), and impairments in endosome retrograde transport in ALS (50). These transport defects can be caused by mutations in kinesins, dynein and tubulin themselves (51–53), as well as adaptors and other RNA binding proteins such as TDP43 and Fus (46).
It will be crucial to determine the mechanisms by which Atx2 can act as a master regulator of the neuronal cytoskeleton. It is known that Atx2 does not associate directly with actin (4), perhaps Atx2 acts indirectly via interaction with actin/microtubule binding proteins, such as profilin, another ALS risk factor which locates to stress granules (54, 55). Another likely option is via regulation of expression of its cognate RNAs – perhaps among these transcripts are known regulators of the actin and microtubule cytoskeleton. Atx2 tightly regulates RNP granules and is necessary for axon path finding (1, 10). It is essential for local translation for synaptic plasticity (2). Ongoing experiments serving to identify Atx2 bound RNAs (TRIBE), along with RNA seq data, will prove indispensable for identifying mechanisms of Atx2 in both neuronal development and neurodegeneration (10).

Currently it is unclear whether the neurodegenerative-related polyQ expansion of Atx2 corresponds to a gain of toxic function or simply to a loss of function of wild type Atx2. Previous reports support both alternatives. For example, protein misfolding and accumulation of Atx2 aggregates induced by polyQ expansion has been linked to the diseases and cell death (56, 57). These phenotypes can be reproduced by knockin of mutant Atx2 in wild type animals, but not by Atx2 knockout mice

(9). In contrast, other works have shown that toxicity of the polyQ Atx2 is independent of its ability to aggregate (58). Our data can't evaluate the potential for gain of toxic of function. However, the neurodevelopmental phenotypes we observe upon Atx2 loss in flies mirror observations in neurodegenerative disease. This may support a potential contribution of loss of functional Atx2 to neurodegeneration. The differences in phenotypes observed in Atx2 knockdown between flies and rodents may be explained by the presence of Atx2-like, a highly homologous gene in rodents (59). Atx2-like might compensate for the loss of function of wild type Atx2 during rodent development. It would be very informative to revisit Atx2 knockout and polyQ knock-in phenotypes in the absence of Atx2-like.

## Materials and Methods

### Fly stocks and plasmids

Fly stocks and crosses were cultured on standard cornmeal food at room temperature based on the Bloomington Stock Center's recipe. Fly stocks can be found in table S1. All experiments used Atx2 shRNA line 44012 unless otherwise stated. For tubulin photoconversion experiments, S2 cells were transfected with pMT-EOS-tubulin described in Barlan et al (60).

### *Drosophila* Cell Culture: Primary Neurons and S2 Cells

*Drosophila* S2 cells were maintained in Insect-Xpress medium (Lonza) at 25°C. These cells came directly from DGRC and their identity was not subsequently confirmed. Transfections were carried out with Effectene (Qiagen) according to the manufacturer's instructions. dsRNA was added to cells on days 1 and 3 and imaging was carried out on day 5. For EB1 experiments a stable S2 cell line was created expressing EB1-GFP under control of the EB1 promoter in the pMT vector. Primary neuronal cultures were prepared by dissection of brains from 3rd instar larvae and dissociation of tissue using liberase (Roche). Cells were plated on ConA coated glass coverslips and maintained in Schneiders medium supplemented with 20% FBS, 5 µg/ml insulin, 100 µg/ml Pen-Strep, 50 µg/ml Gentamycin and 10 µg/ml Tetracycline.

### Survival analysis

For line 44012 (which we designated Atx2 shRNA line 1), homozygous adults were crossed with elav-gal4 flies and number of adults eclosing from pupae cases was counted. For line 36114 (designated Atx2 shRNA line 2), heterozygous adults were crossed with elav-gal4 flies and number of 'non tubby' adults eclosing from pupae cases. Elav-gal4 flies were used as control.

### Immunostaining, Western Blotting and Antibodies

Antibodies and dyes used in this study are detailed in table S2. Full details of immunostaining and Western Blotting can be found in the supplementary information.

### Microscopy and Image Analysis

Full details of microscopy and image analysis can be found in the supplementary information.

### Statistical Analysis

Statistical significance between two groups was determined using the unpaired, nonparametric Mann–Whitney *U* test. Data analyses were performed with Prism v6 (GraphPad Software). Statistical significance is presented as *p<0.05, **p<0.01, ***p<0.001, ****p<0.0001. Data in Figure legends are presented as mean ± standard error.

**Data availability**

All data associated with this work are included in this article and SI Appendix.

**Funding sources and Acknowledgments**

We thank members of the Gelfand lab and Dr. M. Gelfand for helpful discussion. We thank Drs. A. Lim, W. Saxton and S. Rogers for *Drosophila* lines. Research reported in this study was supported by National Institute of General Medical Sciences Grants R01GM052111 and R35GM131752 (to V.I.G.).

**References**

1. B. Bakthavachalu, *et al.*, RNP-Granule Assembly via Ataxin-2 Disordered Domains Is Required for Long-Term Memory and Neurodegeneration. *Neuron* **98**, 754-766.e4 (2018).
2. C. McCann, *et al.*, The ataxin-2 protein is required for microRNA function and synapse-specific long-term olfactory habituation. *Proc. Natl. Acad. Sci. U. S. A.* **108** (2011).
3. I. P. Sudhakaran, *et al.*, FMRP and Ataxin-2 function together in long-term olfactory habituation and neuronal translational control. *Proc. Natl. Acad. Sci. U. S. A.* **111** (2014).
4. T. F. Satterfield, S. M. Jackson, L. J. Pallanck, A drosophila homolog of the polyglutamine disease gene SCA2 is a dosage-sensitive regulator of actin filament formation. *Genetics* **162**, 1687–1702 (2002).
5. D. Lorenzetti, S. Bohlega, H. Y. Zoghbi, The expansion of the CAG repeat in ataxin-2 is a frequent cause of autosomal dominant spinocerebellar ataxia. *Neurology* **49**, 1009–1013 (1997).
6. A. C. Elden, *et al.*, Ataxin-2 intermediate-length polyglutamine expansions are associated with increased risk for ALS. *Nature* **466**, 1069–1075 (2010).
7. K. J. Robinson, M. Watchon, A. S. Laird, Aberrant Cerebellar Circuitry in the Spinocerebellar Ataxias. *Front. Neurosci.* **14** (2020).
8. G. Kim, O. Gautier, E. Tassoni-Tsuchida, X. R. Ma, A. D. Gitler, ALS Genetics: Gains, Losses, and Implications for Future Therapies. *Neuron* (2020) https:/doi.org/10.1016/j.neuron.2020.08.022 (November 5, 2020).
9. T. R. Kiehl, *et al.*, Generation and characterization of Sca2 (ataxin-2) knockout mice. *Biochem. Biophys. Res. Commun.* **339**, 17–24 (2006).
10. A. Singh, *et al.*, ANTAGONISTIC ROLES FOR ATAXIN-2 STRUCTURED AND DISORDERED DOMAINS IN RNP CONDENSATION. *bioRxiv*, 2020.07.02.184796 (2020).
11. T. F. Satterfield, L. J. Pallanck, Ataxin-2 and its Drosophila homolog, ATX2, physically assemble with polyribosomes. *Hum. Mol. Genet.* **15**, 2523–2532 (2006).
12. S. F. Banani, H. O. Lee, A. A. Hyman, M. K. Rosen, Biomolecular condensates: Organizers of cellular biochemistry. *Nat. Rev. Mol. Cell Biol.* **18**, 285–298 (2017).
13. M. D. Stubenvoll, J. C. Medley, M. Irwin, M. H. Song, ATX-2, the C. elegans Ortholog of Human Ataxin-2, Regulates Centrosome Size and Microtubule Dynamics. *PLoS Genet.* **12** (2016).
14. M. M. Gnazzo, *et al.*, The RNA-binding protein ATX-2 regulates cytokinesis through PAR-5 and ZEN-4. *Mol. Biol. Cell* **27**, 3052–3064 (2016).
15. U. del Castillo, *et al.*, Conserved role for Ataxin-2 in mediating endoplasmic reticulum dynamics. *Traffic* **20**, 436–447 (2019).
16. D. A. SHOLL, Dendritic organization in the neurons of the visual and motor cortices of the

cat. *J. Anat.* **87**, 387–406 (1953).
17. U. Del Castillo, W. Lu, M. Winding, M. Lakonishok, V. I. Gelfand, Pavarotti/MKLP1 regulates microtubule sliding and neurite outgrowth in Drosophila neurons. *Curr. Biol.* (2015) https:/doi.org/10.1016/j.cub.2014.11.008.
18. M. Winding, M. T. Kelliher, W. Lu, J. Wildonger, V. I. Gelfand, Role of kinesin-1–based microtubule sliding in *Drosophila* nervous system development. *Proc. Natl. Acad. Sci.* **113**, E4985–E4994 (2016).
19. R. Norkett, U. Del Castillo, W. Lu, V. I. Gelfand, Ser/Thr kinase Trc controls neurite outgrowth in drosophila by modulating microtubule-microtubule sliding. *Elife* **9** (2020).
20. W. Lu, P. Fox, M. Lakonishok, M. W. Davidson, V. I. Gelfand, Initial neurite outgrowth in Drosophila neurons is driven by kinesin-powered microtubule sliding. *Curr. Biol.* **23**, 1018–1023 (2013).
21. W. Yu, *et al.*, Depletion of a microtubule-associated motor protein induces the loss of dendritic identity. *J. Neurosci.* **20**, 5782–91 (2000).
22. U. Del Castillo, H. A. J. Müller, V. I. Gelfand, Kinetochore protein Spindly controls microtubule polarity in Drosophila axons. *Proc. Natl. Acad. Sci. U. S. A.* **117** (2020).
23. A. L. Jolly, *et al.*, Kinesin-1 heavy chain mediates microtubule sliding to drive changes in cell shape. *Proc. Natl. Acad. Sci.* **107**, 12151–12156 (2010).
24. C. Janke, M. M. Magiera, The tubulin code and its role in controlling microtubule properties and functions. *Nat. Rev. Mol. Cell Biol.* **21**, 307–326 (2020).
25. A. Szyk, *et al.*, Molecular basis for age-dependent microtubule acetylation by tubulin acetyltransferase. *Cell* **157**, 1405–1415 (2014).
26. D. Portran, L. Schaedel, Z. Xu, M. Théry, M. V. Nachury, Tubulin acetylation protects long-lived microtubules against mechanical ageing. *Nat. Cell Biol.* **19**, 391–398 (2017).
27. A. Akhmanova, M. O. Steinmetz, Control of microtubule organization and dynamics: Two ends in the limelight. *Nat. Rev. Mol. Cell Biol.* **16**, 711–726 (2015).
28. C. H. Lin, E. M. Espreafico, M. S. Mooseker, P. Forscher, Myosin drives retrograde F-actin flow in neuronal growth cones. *Neuron* **16**, 769–782 (1996).
29. A. E. Twelvetrees, The lifecycle of the neuronal microtubule transport machinery. *Semin. Cell Dev. Biol.* (2020) https:/doi.org/10.1016/j.semcdb.2020.02.008.
30. W. Lu, *et al.*, Competition between kinesin-1 and myosin-v defines drosophila posterior determination. *Elife* **9** (2020).
31. L. C. Kapitein, *et al.*, Myosin-V opposes microtubule-based cargo transport and drives directional motility on cortical actin. *Curr. Biol.* **23**, 828–834 (2013).
32. K. J. De Vos, M. Hafezparast, Neurobiology of axonal transport defects in motor neuron diseases: Opportunities for translational research? *Neurobiol. Dis.* **105**, 283–299 (2017).
33. I. Noordstra, *et al.*, Control of apico–basal epithelial polarity by the microtubule minus-end-binding protein CAMSAP3 and spectraplakin ACF7. *J. Cell Sci.* **129**, 4278–4288 (2016).
34. R. Banerjee, J. A. White, S. Gunawardena, “In vivo visualization of moving synaptic cargo complexes within Drosophila larval segmental axons” in *Methods in Molecular Biology*, (Humana Press Inc., 2020), pp. 293–300.
35. W. Lu, P. Fox, M. Lakonishok, M. W. Davidson, V. I. Gelfand, Initial neurite outgrowth in drosophila neurons is driven by kinesin-powered microtubule sliding. *Curr. Biol.* **23**, 1018–1023 (2013).
36. R. Norkett, U. Del Castillo, W. Lu, V. I. Gelfand, Ser/Thr kinase Trc controls neurite outgrowth in Drosophila by modulating microtubule-microtubule sliding. *Elife* **9** (2020).
37. U. Del Castillo, R. Norkett, V. I. Gelfand, Unconventional Roles of Cytoskeletal Mitotic Machinery in Neurodevelopment. *Trends Cell Biol.* **29**, 901–911 (2019).
38. S. Lin, M. Liu, O. I. Mozgova, W. Yu, P. W. Baas, Mitotic Motors Coregulate Microtubule Patterns in Axons and Dendrites. *J. Neurosci.* **32**, 14033–14049 (2012).
39. Y. Zheng, *et al.*, Dynein is required for polarized dendritic transport and uniform microtubule orientation in axons. *Nat. Cell Biol.* **10**, 1172–1180 (2008).
40. D. H. Roossien, P. Lamoureux, K. E. Miller, Cytoplasmic dynein pushes the cytoskeletal meshwork forward during axonal elongation. *J. Cell Sci.* **127**, 3593–3602 (2014).
41. M. J. Papandréou, C. Leterrier, The functional architecture of axonal actin. *Mol. Cell. Neurosci.* **91**, 151–159 (2018).

42. I. Hahn, *et al.*, Tau, XMAP215/Msps and Eb1 jointly regulate microtubule polymerisation and bundle formation in axons. *bioRxiv*, 2020.08.19.257808 (2020).
43. F. Bradke, C. C. Dotti, The role of local actin instability in axon formation. *Science (80-. ).* **283**, 1931–1934 (1999).
44. F. Korobova, T. Svitkina, Arp2/3 complex is important for filopodia formation, growth cone motility, and neuritogenesis in neuronal cells. *Mol. Biol. Cell* **19**, 1561–1574 (2008).
45. A. W. Schaefer, *et al.*, Coordination of Actin Filament and Microtubule Dynamics during Neurite Outgrowth. *Dev. Cell* **15**, 146–162 (2008).
46. V. K. Godena, *et al.*, Increasing microtubule acetylation rescues axonal transport and locomotor deficits caused by LRRK2 Roc-COR domain mutations. *Nat. Commun.* **5**, 1–11 (2014).
47. N. Kaul, V. Soppina, K. J. Verhey, Effects of α-tubulin K40 acetylation and detyrosination on kinesin-1 motility in a purified system. *Biophys. J.* **106**, 2636–2643 (2014).
48. J. C. Fiala, M. Feinberg, A. Peters, H. Barbas, Mitochondrial degeneration in dystrophic neurites of senile plaques may lead to extracellular deposition of fine filaments. *Brain Struct. Funct.* **212**, 195–207 (2007).
49. S. C. Correia, G. Perry, P. I. Moreira, Mitochondrial traffic jams in Alzheimer's disease - pinpointing the roadblocks. *Biochim. Biophys. Acta - Mol. Basis Dis.* **1862**, 1909–1917 (2016).
50. Y. Xie, *et al.*, Endolysosomal Deficits Augment Mitochondria Pathology in Spinal Motor Neurons of Asymptomatic fALS Mice. *Neuron* **87**, 355–370 (2015).
51. N. Hirokawa, Y. Tanaka, Kinesin superfamily proteins (KIFs): Various functions and their relevance for important phenomena in life and diseases. *Exp. Cell Res.* **334**, 16–25 (2015).
52. S. L. Reck-Peterson, W. B. Redwine, R. D. Vale, A. P. Carter, The cytoplasmic dynein transport machinery and its many cargoes. *Nat. Rev. Mol. Cell Biol.* **19**, 382–398 (2018).
53. M. A. Tischfield, *et al.*, Human TUBB3 Mutations Perturb Microtubule Dynamics, Kinesin Interactions, and Axon Guidance. *Cell* **140**, 74–87 (2010).
54. M. Ralser, *et al.*, Ataxin-2 and huntingtin interact with endophilin-A complexes to function in plastin-associated pathways. *Hum. Mol. Genet.* **14**, 2893–2909 (2005).
55. M. D. Figley, G. Bieri, R.-M. Kolaitis, J. P. Taylor, A. D. Gitler, Neurobiology of Disease Profilin 1 Associates with Stress Granules and ALS-Linked Mutations Alter Stress Granule Dynamics (2014) https:/doi.org/10.1523/JNEUROSCI.0543-14.2014.
56. S. W. Davies, *et al.*, Formation of neuronal intranuclear inclusions underlies the neurological dysfunction in mice transgenic for the HD mutation. *Cell* **90**, 537–548 (1997).
57. L. T. Pflieger, *et al.*, Gene co-expression network analysis for identifying modules and functionally enriched pathways in SCA2. *Hum. Mol. Genet.* **26**, 3069–3080 (2017).
58. D. P. Huynh, K. Figueroa, N. Hoang, S. M. Pulst, Nuclear localization or inclusion body formation of ataxin-2 are not necessary for SCA2 pathogenesis in mouse or human. *Nat. Genet.* **26**, 44–50 (2000).
59. C. Kaehler, *et al.*, Ataxin-2-Like Is a Regulator of Stress Granules and Processing Bodies. *PLoS One* **7** (2012).
60. K. Barlan, W. Lu, V. I. Gelfand, The Microtubule-Binding Protein Ensconsin Is an Essential Cofactor of Kinesin-1. *Curr. Biol.* **23**, 317–322 (2013).

## Figure 1

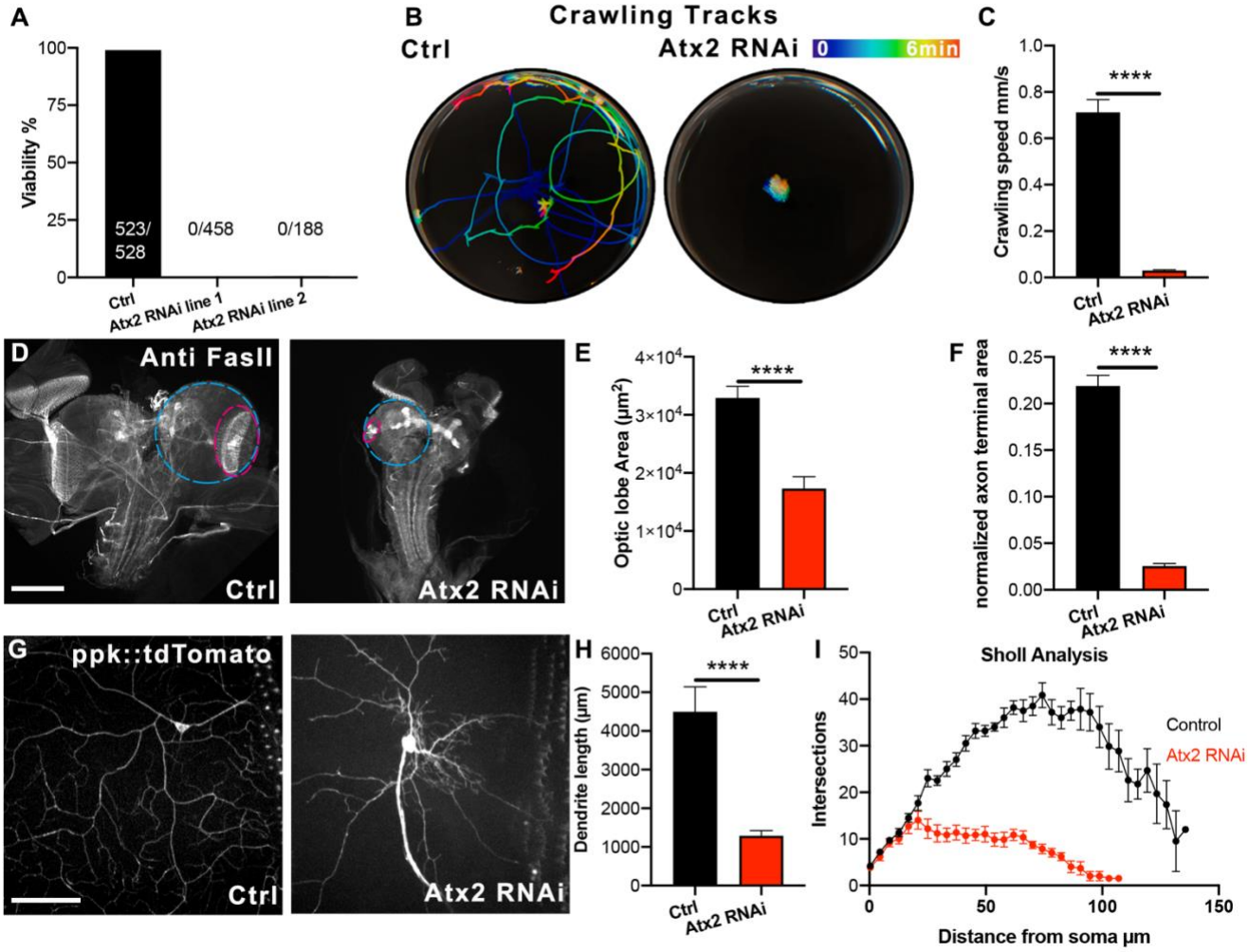


Figure 1: Ataxin-2 is essential for neurodevelopment, locomotion and viability in *Drosophila.*

A. Atx2 depletion is lethal at the pupae stage. Percentage of adults eclosing from pupae cases (Control = 99%, Atx2 RNAi line 1 = 0.0%, Atx2 RNAi line 2 = 0.0%). B. Atx2 depletion impairs locomotion. Example crawling tracks of control and elav>Atx2 RNAi 3rd instar larvae. C. Crawling velocity of control and elav>Atx2 RNAi 3rd instar larvae (Control = 0.71 mm/s ± 0.05, Atx2 RNAi = 0.03 mm/s ± 0.003). D. Atx2 depletion decreases brain size and innervation. Example images of control and elav>Atx2 RNAi brains from *Drosophila* 3rd instar larvae. Scale bar, 100µm. E. Size of optic lobes in control and elav>Atx2 RNAi brains (Control = 32931 $\mu m^2$ ± 1993, Atx2 RNAi = 17306 $\mu m^2$ ± 2028, n=18 control and 9 Atx2 RNAi brains, $p<0.0001$). F. Area of optic stalks normalized to optic lobes in control and Atx2 RNAi brains (Control = 0.212 ± 0.01, Atx2 RNAi = 0.026 ± 0.003, n=18 control and 9 Atx2 RNAi brains, $p<0.0001$). G. Atx2 depletion decreases dendrite development. Example images of DA neurons in control and elav>Atx2 RNAi neurons. Scale bar, 50µm. H. Dendrite length per cell in control and elav>Atx2 RNAi neurons (Control = 4500 µm ± 644, Atx2 RNAi = 1290 µm ± 134, n=11 animals). I. Sholl analysis of control and Atx2 RNAi neurons DA neurons showing number of intersections with distance from soma.

## Figure 2

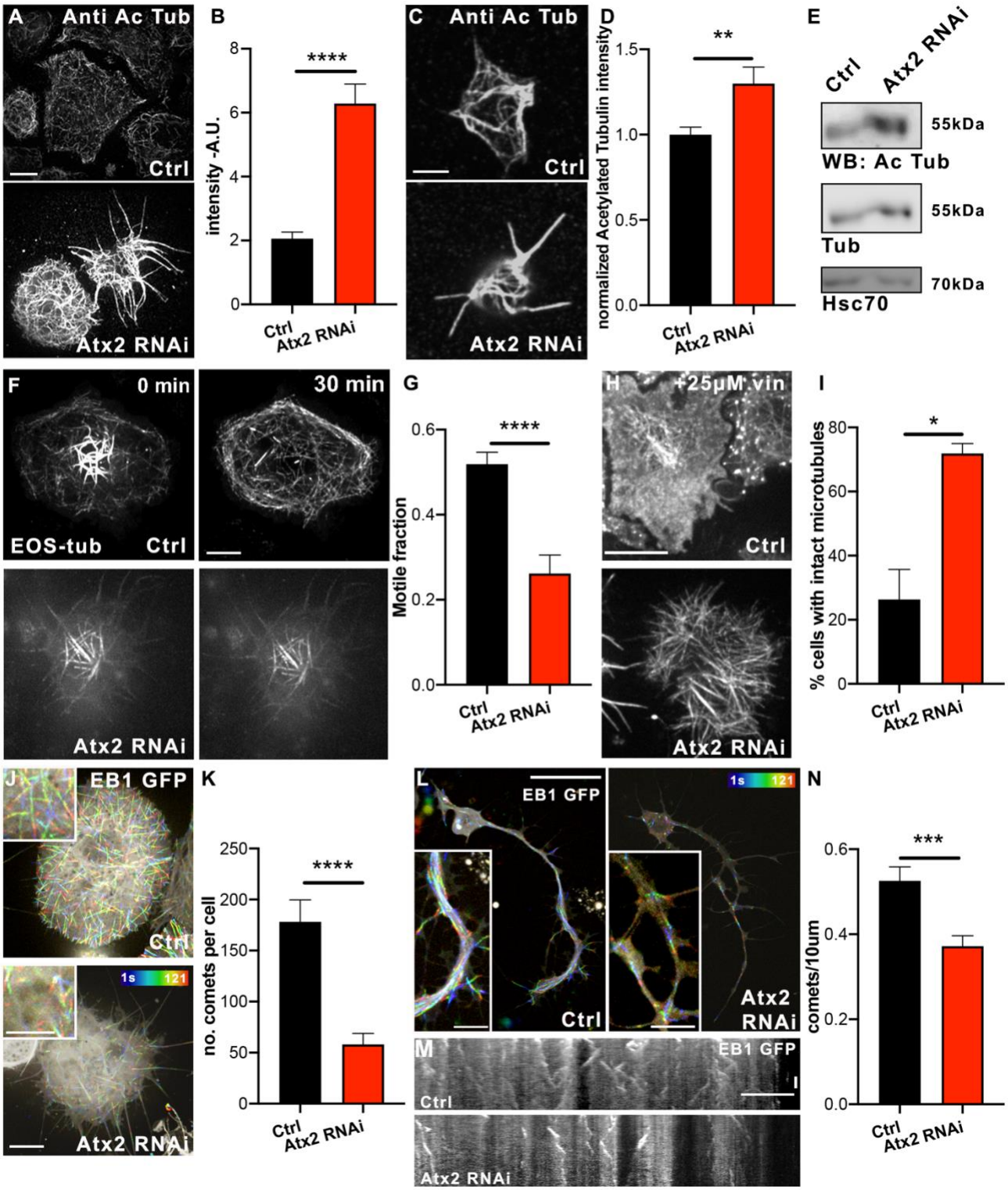
A
Anti Ac Tub
Ctrl
Atx2 RNAi
B
****
intensity -A.U.
8
6
4
2
0
Ctrl
Atx2 RNAi
C
Anti Ac Tub
Ctrl
Atx2 RNAi
D
**
normalized Acetylated Tubulin intensity
1.5
1.0
0.5
0.0
Ctrl
Atx2 RNAi
E
Ctrl
Atx2 RNAi
55kDa
WB: Ac Tub
55kDa
Tub
70kDa
Hsc70
F
0 min
30 min
EOS-tub
Ctrl
Atx2 RNAi
G
****
Motile fraction
0.6
0.4
0.2
0.0
Ctrl
Atx2 RNAi
H
+25μM vin
Ctrl
Atx2 RNAi
I
*
% cells with intact microtubules
80
60
40
20
0
Ctrl
Atx2 RNAi
J
EB1 GFP
Ctrl
1s
121
Atx2 RNAi
K
****
no. comets per cell
250
200
150
100
50
0
Ctrl
Atx2 RNAi
L
EB1 GFP
Ctrl
1s
121
Atx2 RNAi
M
EB1 GFP
Ctrl
Atx2 RNAi
N
***
comets/10um
0.6
0.4
0.2
0.0
Ctrl
Atx2 RNAi

5

Figure 2: Ataxin-2 depletion decreases microtubule dynamics.

A. Example images showing Atx2 depletion in *Drosophila* S2 cells increases microtubule acetylation as quantified in B (Signal intensity Control = 2061210 ± 204596 A.U. Atx2 RNAi = 6286404 ± 608574). C. Example images showing Atx2 depletion increases microtubule acetylation in *Drosophila* neurons in culture (scale bar, 10µm), as quantified in D (Signal Intensity Control = 1.0 ± 0.04, n = 23 cells, Signal Intensity Atx2 RNAi = 1.3 ± 0.10, n = 27 cells, p = 0.01). E. Western blot of Acetylated tubulin levels in Control and Atx2 RNAi brain lysate from *Drosophila* 3$^{rd}$ instar larvae. F. Example images of EOS-tubulin in S2 cells 0 and 30mins after photoconversion (scale bar, 10µm) as quantified in G (Motile fraction Control = 0.52 ± 0.03, n = 21 cells, Atx2 RNAi = 0.26s ± 0.04, n = 22 cells, p < 0.0001). H. Example images of tubulin staining in S2 cells showing microtubules after 25µM vinblastine treatment 1hr. Scale bar, 10µm. I. Quantification of cells with an intact microtubule network after vinblastine treatment (Control = 26.4% ± 9.4, Atx2 RNAi = 71.9% ± 3.1). J. Temporal color code images showing motility of EB1-GFP comets in S2 cells over 120 seconds. Scale bar, 10µm. K. Quantification of number of EB1 comets per cell. L. Temporal color code images showing motility of EB1-GFP comets in cultured neurons over 120 seconds. Scale bar, 10µm, inset, 5µm. M. Kymographs showing motility of comets in neuronal processes over 120 seconds. Scale bar, 10µm. N. Quantification of number of EB1 comets per process length (Control = 0.53 ± 0.03, n=31, Atx2 RNAi = 0.37 ± 0.02, n=34, p = 0.0004).

## Figure 3

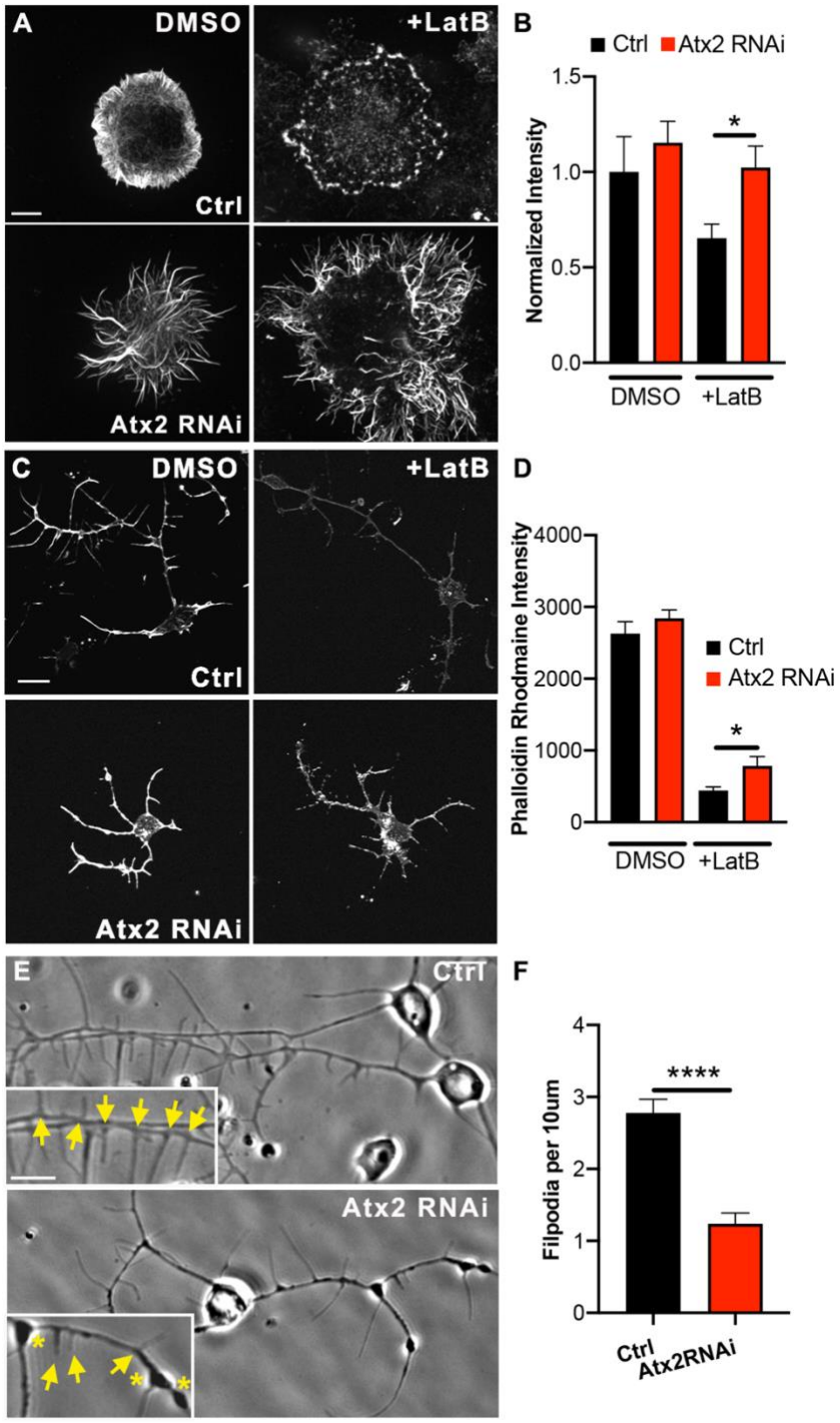
A
DMSO
+LatB
Ctrl
Atx2 RNAi
B
Ctrl
Atx2 RNAi
Normalized Intensity
1.5
1.0
0.5
0.0
*
DMSO
+LatB
C
DMSO
+LatB
Ctrl
Atx2 RNAi
D
Phalloidin Rhodmaine Intensity
4000
3000
2000
1000
0
Ctrl
Atx2 RNAi
*
DMSO
+LatB
E
Ctrl
Atx2 RNAi
F
Filpodia per 10um
4
3
2
1
0
****
Ctrl
Atx2RNAi

586

Figure 3: Ataxin-2 depletion stabilizes the actin cytoskeleton

A. Example images showing phalloidin staining for F-actin in control and Atx2 RNAi treated *Drosophila* S2 cells treated with DMSO or 10µM LatB for 1hr. Scale bar, 10µm B. Normalized Phalloidin Rhodamine signal (Control = 1.00 ± 0.19, Atx2 RNAi = 1.15 ± 0.11, Control + LatB = 0.65 ± 0.07, Atx2 RNAi + LatB = 1.02 ± 0.11, n = 15-24 cells, p = 0.03). C. Example images showing phalloidin staining in control and Atx2 RNAi neurons treated with DMSO or 10µM LatB for 1hr. Scale bar, 10µm. D. Quantification of Phalloidin Rhodamine intensity along length of neuron (Signal Intensity Control LatB = 440.4 ± 53, n = 37 cells, Signal Intensity Atx2 RNAi LatB = 786.5 ± 128, n = 27 cells, p = 0.02). E. Example phase contrast images showing filipodia from neuronal processes in control and Atx2 RNAi neurons. Scale bar, 10µm. F. Average number of filopodia per 10µm process length (Control = 2.8 ± 0.19, n = 28 cells, Atx2 RNAi = 1.2 ± 0.15, n = 28 cells, p <0.0001).

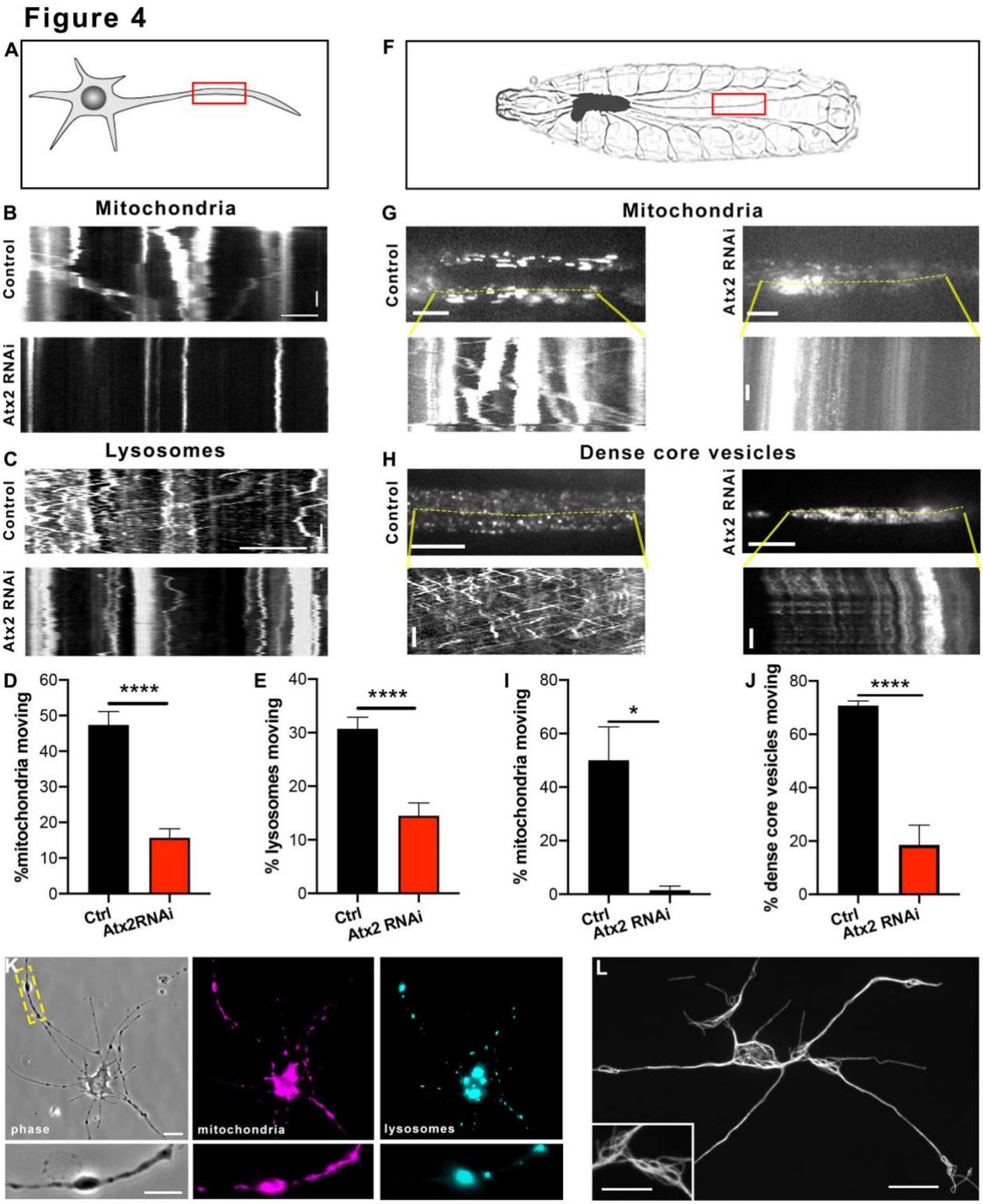


Figure 4: Ataxin-2 depletion inhibits organelle transport

A. Schematic showing region of imaging in neurons in culture. B. Example kymographs showing mitochondria motility in processes of control and Atx2 RNAi neurons. Horizontal scale bar, 10µm.

Vertical scale bar, 20s. C. Example kymographs showing lysosome motility in processes of control and Atx2 RNAi neurons. Horizontal scale bar, 10µm. Vertical scale bar, 20s. D. Quantification of motile mitochondria in control and Atx2 knockdown neurons (Control = 47% ± 3.7, n = 25 cells, Atx2 RNAi = 15.7% ± 2.5, n = 28 cells, $p < 0.0001$). E. Quantification of motile lysosomes in control and Atx2 knockdown neurons (Control = 31% ± 2.1, n = 25 cells, Atx2 RNAi = 14.5% ± 2.4, n = 29 cells, $p < 0.0001$). F. Schematic image of a third instar larva showing segmental nerves. Example kymographs showing mitochondria motility (G) and dense core vesicle motility (H) in segmental nerves *in vivo* in control and Atx2 RNAi larvae. Vertical scale bars, 10s, horizontal scale bars,10µm for dense core vesicles, 20µm for mitochondria. I. Quantification of motile mitochondria in control and Atx2 knockdown segmental nerves *in vivo* (Control = 50% ± 12.5, n = 3 larvae, Atx2 RNAi = 1.5% ± 1.5, n = 3 larvae, $p = 0.015$). J. Quantification of motile DCVs in control and Atx2 knockdown segmental nerves *in vivo* (Control = 66% ± 1.7, n = 9 larvae, Atx2 RNAi = 18.6% ± 7.4, n = 8 larvae, $p < 0.0001$). K. Example image showing mitochondria and lysosome distribution in Atx2 RNAi cultured neuron. Scale bar, 10µm, inset 5µm. L. Example super resolution images of microtubules in varicosities in Atx2 RNAi neurons. Scale bars, 10µm.

Supplementary Information for

**Ataxin-2 is essential for neurodevelopment in *Drosophila* and is a major regulator of the cytoskeleton**

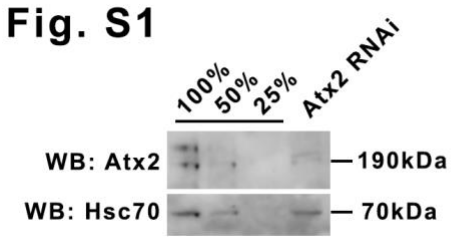


Fig. S1: Ataxin-2 depletion in brains by western blot. Western blot demonstrating knockdown of Atx2 by elav>Atx2 shRNA #44012.

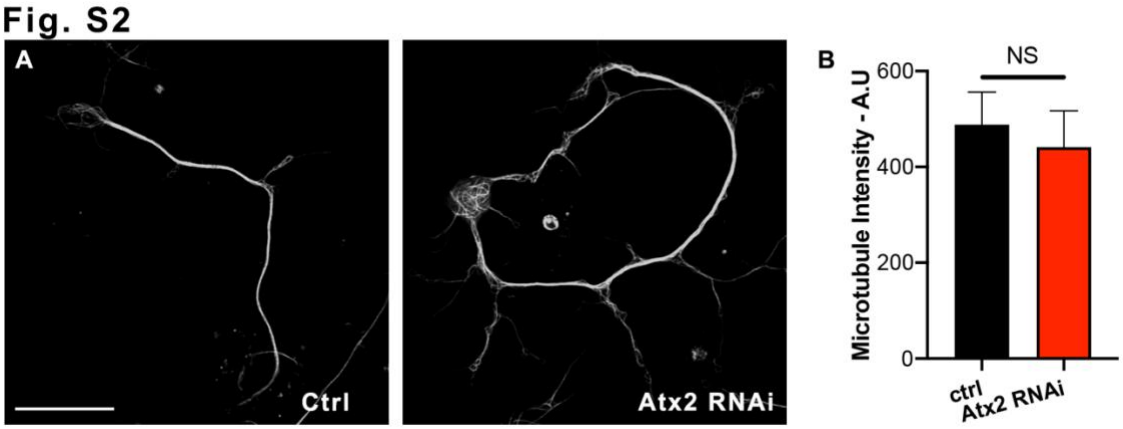


Fig. S2: Microtubule content is equal control vs Atx2 RNAi neurons in culture. A. Example images showing tubulin staining in extracted neurons. Scale bar, 20µm. B. Quantification of tubulin signal intensity (Ctrl = 488.4 ± 67.7, n = 8 cells, Atx2 RNAi = 441.2 ± 76.1, n = 6 cells, NS p = 0.85)

# Supplementary methods

## Immunostaining, Western Blotting and Antibodies

Optic lobes, dissected from third-instar larva in 1 × PBS, were fixed in 4% (wt/wt) formaldehyde (methanol-free) in PBT (1 × PBS, 0.1% Triton X-100) for 20 min; brains were washed five times with PBTB (PBT + 0.2% bovine serum albumin) for 10 min and blocked in 5% (vol/vol) normal goat serum for 1 h. Samples were incubated with primary anti-Fasciclin II antibody (1:40) at 4° C overnight, washed and incubated with secondary anti-mouse for 2h at room temperature (RT). Finally, samples were washed with PBT for 10min five times before mounting.
For immunostaining of S2 cells and cultured neurons, cells were fixed 5 mins in methanol (S2 cells) or 1% glutaraldehyde and quenched in 2 mg/ml sodium borohydride (neurons). Cells were permeabilised and blocked in wash buffer (1% BSA, 0.1% Triton X-100 in TBS) for 30mins and incubated with primary antibody in wash buffer (Anti-Acetylated tubulin 1:100-1:250, DM1a 1:1000). Coverslips were washed 3x in wash buffer and incubated with secondary antibodies (1:200). For extraction, cells were incubated in extraction buffer (1% Triton X-100, 1uM taxol, 30% glycerol in BRB-80) for 2 minutes, then in extraction buffer with 1% glutaraldehyde for 2 minutes, then 1% glutaraldehyde in PBS for 3 minutes followed by reduction as above. For western blotting, dissected third instar larvae brains or S2 cell lysate were prepared in 1% SDS, boiled in laemmli buffer and analyzed by SDS-PAGE.

## Microscopy and Image Analysis

To image DA neurons or S2 cells we used a Nikon Eclipse U2000 inverted microscope equipped with a Yokogawa CSU10 spinning disk head with a perfect focus system and a 40x 1.30 or 100x 1.45 oil immersion lens, using Evolve EMCCD (Photometrics) and controlled by Nikon Elements 4.00.07 software. For EB1 imaging in S2 cells images were acquired at 1 fps. For organelle imaging in larvae, larvae were immobilised and frames were acquisition was at 3 fps (dense core vesicles) or 0.5 fps (mitochondria). Immunostained brains and neurons were imaged on a Nikon Ti2 inverted microscope equipped with W1 spinning disk driven by Nikon Elements 5.20 using a 20X or 100x 1.45 oil immersion lens and CMOS prime 95B sensor (Photometrics). For microtubule organization images, this set-up was used with a Live-SR (Gataca systems). Live imaging of lysosomes and EB1 comets in neurons was carried out at 1fps. For photoconversion experiments we applied 405 nm light from a light-emitting diode light source (89 North Heliophor) for 5 s, using an adjustable diaphragm to constrain light and illuminate only a specific region of interest. After photoconversion, images were collected every ten minutes for 30 minutes. Imaging of filopodia, organelle distribution in culture and mitochondrial trafficking was carried out on a Nikon Ti inverted microscope with a Hamamatsu Orca Flash sensor. For locomotion assays, 3$^{rd}$ Instar larvae were allowed to crawl on the surface of a petri dish containing 2% agarose supplemented with apple juice and charcoal powder. Trajectories are presented using the Physics Temporal-Color Code plugin in Fiji.

Image analysis was carried out in Fiji unless otherwise stated. Total neurite length in DA neurons was measured using the ‘curve tracing’ and sholl analysis plugins. Tubulin motile fraction was calculated as ‘photoconverted signal outside original photoconversion zone / original photoconverted signal’ at 30mins post photoconversion. Numbers and motility of EB1 comets, mitochondria and lysosomes in culture or *in vivo* was carried out by generating kymographs and analyzed using the ‘kymobutler’ software (1). Motile organelles were defined as those that moved more than 2µm over the course of the movie. Comets that moved more than 1µm over the course

of the movie were counted. EB1 comets in S2 cells were counted using Nikon elements analysis software (v5.20). Numbers of filopodia and organelles in varicosities were scored manually.

Table S1: Fly stocks and sources used in this study.

| Line | Identifier | Source |
|---|---|---|
| Ataxin-2 RNAi TRiP line #1 (Val20, second chromosome attP40 insertion targeting CDS 561-581) | 44012 | Bloomington Drosophila Stock Center (BDSC) |
| Ataxin-2 RNAi TRiP line #2 (Val20, third chromosome attP2 insertion targeting Atx2 CDS 474-494) | 36114 | BDSC |
| elav-gal4 | 8760 | BDSC |
| ppk-CD4-tomato | 35844 | BDSC |
| UASt-mCherry.mito.OMM | 66532 | BDSC |
| Ubi-EB1-GFP | | S. Rogers |
| D42 gal4>UAS ANF GFP | | A. Lim, W. Saxton (2) |

Table S2: Antibodies used in this study.

| Antibody | Source | Concentration |
|---|---|---|
| Anti FasII 1D4 | DSHB | 1:40 |
| Anti Acetylated alpha tubulin (K40) | protein tech 66200 | 1:100-1:250 |
| Anti alpha tubulin DM1a | Prepared in house | 1:1000 |
| Anti tubulin rb polyclonal | made in house | 1:1000 |
| Anti Hsc 70 K-19 | Santa Cruz | 1:200 |
| HRP-conjugated anti mouse | Jackson | 1:10,000 |
| HRP-conjugated anti rabbit | Jackson | 1:10,000 |
| HRP-conjugated anti goat | Jackson | 1:10,000 |
| Alexafluor 647 conjugated anti mouse IgG | Jackson | 1:250 |
| Lysotracker DND 99 | Invitrogen | 1:10,000 |

| | | |
|---|---|---|
| Rhodamine conjugated Phalloidin | Jackson | 1:1000 |

## Video Legends

Movie 1: Crawling behavior of control (elav-gal4) and Atx2 RNAi (elav>Atx2 RNAi) *Drosophila* 3rd Instar Larvae, Related to Figure 1B.

Movie 2: Time-lapse of control (untreated cell) or Atx2 RNAi S2 cells expressing EOS-tub. Scale bar, 10μm. Related to Fig. 2F.

Movie 3: Time-lapse of control (untreated cell) or Atx2 RNAi S2 cells expressing EB1-GFP. Scale bar, 10μm. Related to Fig. 2J.

Movie 4: Time-lapse of primary neurons expressing EB1-GFP of two different genotypes. Control (elav-gal4) and Atx2 RNAi (elav>Atx2 RNAi). Scale bar, 10μm. Related to Fig. 2L.

Movie 5: Transport of mitochondria in primary cultures of control and Atx2 RNAi expressing MitomCherry. Scale bar, 10μm. Related to Fig. 4B.

Movie 6: Transport of lysosomes in primary cultures of control and Atx2 RNAi labelled with lysotracker. Scale bar, 10μm. Related to Fig. 4C.

Movie 7: Transport of mitochondria in motor segmental nerves of control and Atx2 RNAi expressing mitoGFP. Scale bar, 10μm. Related to Fig. 4G.

Movie 8: Transport of Dense core vesicles in motor segmental nerves of control and Atx2 RNAi expressing ANF-GFP. Scale bar, 10μm. Related to Fig. 4G.

Supplementary References

1. M. A. Jakobs, A. Dimitracopoulos, K. Franze, Kymobutler, a deep learning software for automated kymograph analysis. *Elife* **8** (2019).
2. A. Lim, A. Rechtsteiner, W. M. Saxton, Two kinesins drive anterograde neuropeptide transport. *Mol. Biol. Cell* **28**, 3542–3553 (2017).